

## A 3D Broadband Seismometer Array Experiment at the Homestake Mine

by Vuk Mandic, Victor C. Tsai, Gary L. Pavlis, Tanner Prestegard, Daniel C. Bowden, Patrick Meyers, and Ross Caton

### ABSTRACT

Seismometer deployments are often confined to near the Earth's surface for practical reasons, despite the clear advantages of deeper seismometer installations related to lower noise levels and more homogeneous conditions. Here, we describe a 3D broadband seismometer array deployed at the inactive Homestake Mine in South Dakota, which takes advantage of infrastructure originally setup for mining and is now used for a range of scientific experiments. The array consists of 24 stations, of which 15 were underground, with depths ranging from 300 ft (91 m) to 4850 ft (1478 m), and with a 3D aperture of  $\sim 1.5$  km in each direction, thus spanning a 3D volume of about  $3.4$  km<sup>3</sup>. We describe unique research opportunities and challenges related to the 3D geometry, including the generally low ambient noise levels, the strong coherency between observed event waveforms across the array, and the technical challenges of running the network. This article summarizes preliminary results obtained using data acquired by the Homestake array, illustrating the range of possible studies supported by the data.

*Electronic Supplement:* A 3D image of the seismic array implemented at Homestake, along with the existing drifts and shafts in the mine, and the local topography.

### INTRODUCTION

Seismology has been a ubiquitous tool for determining Earth structure and learning about various dynamic sources, including earthquakes and nuclear explosions (Lay and Wallace, 1995; Rost and Thomas, 2002; Stein and Wysession, 2003). The number of seismic stations has grown appreciably in the past few decades, with more than 7000 broadband seismometers deployed within the United States alone and more than

20,000 worldwide (Incorporated Research Institutions for Seismology [IRIS], 2017). However, despite this large number of seismometers, instruments have largely been confined to the Earth's surface, with few stations having been placed at depths greater than 100 m, primarily because of the practical difficulty and cost of getting to such depths. The exceptions have been limited to isolated boreholes (e.g., Abercrombie, 1995; Ma *et al.*, 2012), the Parkfield borehole arrays (e.g., Nadeau and McEvilly, 1997), the Hi-net array (e.g., Okada *et al.*, 2004), the UNDERSEIS array (Saccorotti *et al.*, 2006), the LSBB array (Gaffet *et al.*, 2009), and in active mines (Gibowicz *et al.*, 1991; Richardson and Jordan, 2002), usually limited to high-frequency geophones rather than more broadband seismometers. This article describes a new high-density broadband array deployed across a range of depths down to nearly 1500 m.

Although observing ground motions at or near the Earth's surface has generally been acceptable, there are a number of reasons why observations at deeper depths, particularly from an array of instruments, would potentially be useful. It is well known that most seismic noise is generated near the surface and that this noise generally decreases significantly with depth (Levin and Lynn, 1958; Forbes, 1965; Green, 1965; McNamara and Buland, 2004). Because the instrument noise in modern seismometers is typically smaller than the seismic noise, observations at depth have the potential to have higher signal-to-noise (SNR) ratios and therefore may more accurately measure the elastic waves arriving from any source. The second main reason that seismic measurements at depth could be advantageous is that the weathered near-surface layers add additional heterogeneity to shallow structure (e.g., Boore and Joyner, 1997). The weathered layer universally has slower seismic velocities, and the heterogeneity caused by variability in weathering makes it nearly always a strongly scattering medium. Because nearly all observations contain this complexity, it is often challenging to estimate the magnitude of this effect, but it is expected that observations far away from such heterogeneities are simpler and more predictable. Data from the experiment described here have potential for improving insights on the near-surface scattering problem.

In addition to illuminating fundamental questions on seismic wave propagation, seismic measurements at depth are also of interest in the field of gravitational-wave astrophysics.

The Laser Interferometer Gravitational-Wave Observatory recently announced the first direct detections of gravitational waves produced in a merger of binary black hole systems (Abbott *et al.*, 2016a,b), hence ushering a new field of inquiry in astrophysics. To fully explore the scientific potential of this field, more sensitive detectors are being designed such as the Einstein Telescope (Punturo *et al.*, 2010), the Cosmic Explorer (Abbott *et al.*, 2017), and the Matter-wave laser Interferometric Gravitation Antenna (Canuel *et al.*, 2016). One of the limiting noise factors in these detectors at frequencies below 10 Hz is the seismic noise that causes fluctuations in the local gravitational field. It is expected that this noise source will be reduced underground because of the suppression of seismic surface waves. Underground seismic measurements are therefore needed to quantify this attenuation factor and its depth dependence, thereby directly informing the design of future generations of gravitational-wave detectors.

To explore the promise of subsurface seismological observations, both for geophysical and astrophysical applications, we built and operated an underground 3D array at the Homestake Mine in Lead, South Dakota. Homestake was one of the largest and deepest gold mines in North America. It officially closed operations in 2002 but reopened in 2007 as the Sanford Underground Research Facility (SURF) and currently supports several other experiments, including dark matter and neutrino experiments that benefit from the cosmic ray shielding of the rock overburden. A precursor of the array described here was one of the first scientific endeavors at the Homestake Mine after it reopened in 2007 (Harms *et al.*, 2010). The significant infrastructure in the Homestake Mine, including easy access to numerous underground levels with hundreds of kilometers of available drifts, some provided with power and digital network infrastructure, and safety protocols and the SURF infrastructure made the Homestake Mine a well-suited location for the development of a 3D seismometer array.

In this article, we describe the novelty of the 3D Homestake array compared with other subsurface seismological deployments, the experience learned in operating the underground array for 2 yrs, and preliminary results that demonstrate the potential of these data for additional research in the future.

## SEISMOMETER ARRAY

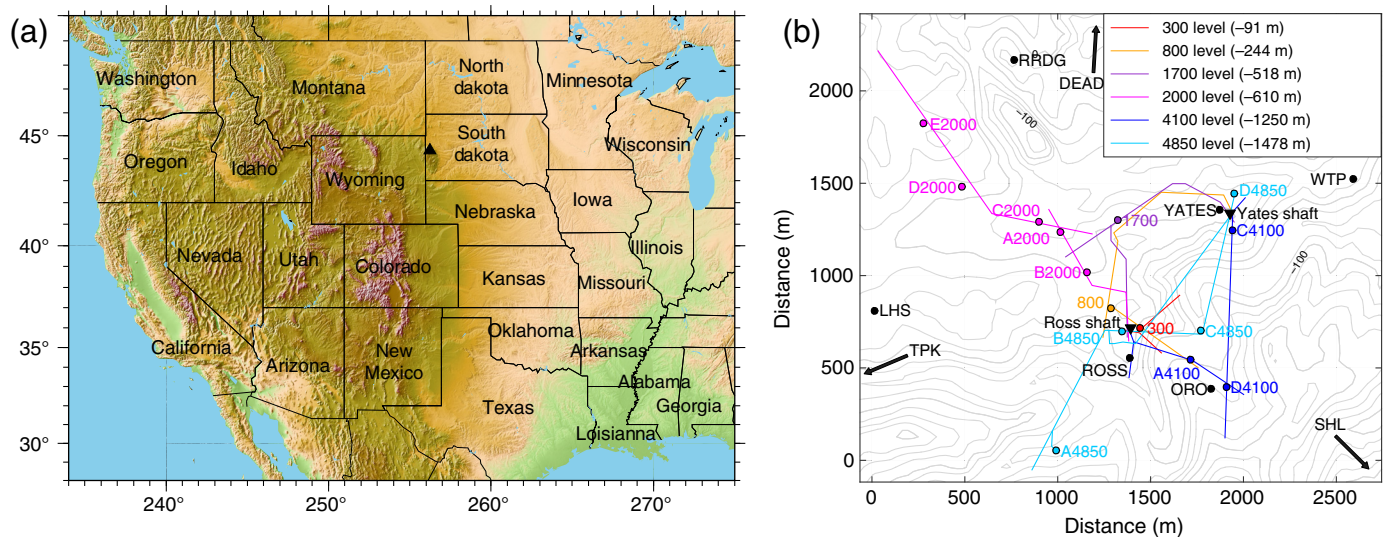
The Homestake seismometer array, depicted in Figure 1, consisted of 24 seismic stations: 15 stations underground and 9 on the surface. The locations of stations are known with uncertainties on the order of 1 m based on precise surveys for past mining operations provided by SURF. Underground station locations were obtained from these maps. Surface station coordinates come from long-term averages of Global Positioning System (GPS) data. All of the underground stations of this array were installed between December 2014 and March 2015 and remained operational until December 2016. The surface stations were installed in May 2015 and remained operational until September 2016. The seismic equipment used in

the experiment was provided by the Program for the Array Seismic Studies of the Continental Lithosphere (PASSCAL) instrument center, which is a part of IRIS. Most stations used Streckheisen STS-2 high-sensitivity broadband seismometers. The exceptions were the underground station on the 300-ft level and three surface stations, where we deployed the more water-resistant Güralp CMG-3T seismometers.

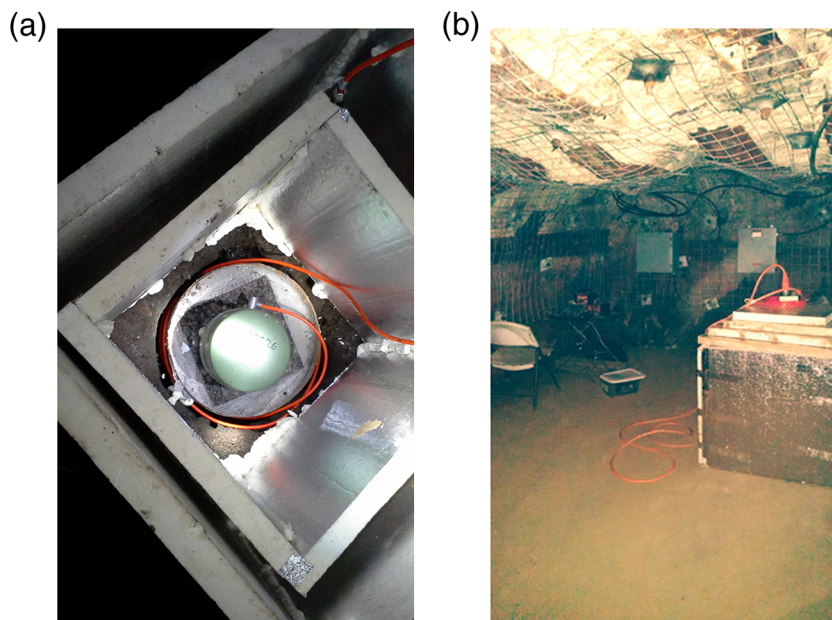
The underground stations were scattered across several levels: one at a depth of 300 ft (91 m), one at 800 ft (244 m), one at 1700 ft (518 m), five at 2000 ft (610 m), three at 4100 ft (1250 m), and four at 4850 ft (1478 m). The locations of these stations were chosen to maximize the horizontal aperture of the array within the constraints imposed by safe access, availability of power, and access to SURF's fiberoptic network. To illustrate the beamforming ability of this array, the array's aperture of 1.5 km in depth will enable slowness estimates for wavelengths of about 0.5 km or less, which for a vertically traveling *P* wave at 5 km/s implies frequencies of 10 Hz and above. Lower frequencies would be accessible in horizontal directions because of the larger horizontal extent of the array. Similarly, lower frequencies of *S* waves and surface waves could also be studied.

We strove to locate sites as far as possible from activity in the mine and from water drainage pathways. Stations were usually placed in alcoves or blind alleys to minimize the effects of the air drifts, although several stations were installed in enlarged areas within the main drifts of the mine. In most cases, we found there were complex trade-offs between cost of installation and distance from active operations. Many sites had existing concrete pads of various sizes and thicknesses from the original mine operation. When necessary, we poured a concrete pad directly onto the bedrock. In all cases, a granite tile was attached to the pad using thinset mortar. All underground site preparation was completed three (or more) months prior to the installation of the instruments. Each seismometer was placed directly onto the granite tile and was oriented to cardinal directions using an Octans gyrocompass from the IRIS-PASSCAL instrument center (Ekström and Busby, 2008), resulting in better than 1° orientation precision. To reduce noise induced by air flow, we covered each sensor with two nested huts constructed of 2-inch-thick polyisocyanurate foam panels and sealed with foam sealant, following Harms *et al.* (2010; see Fig. 2a). The digitizer was placed several meters away and included a Quanterra Q330 data logger operating at a sampling rate of 100 Hz, a data storage baler, and network and power supply electronics, as depicted in Figure 2b. Each station was powered by a small 12V battery continuously recharged by an a.c. charger. The battery provided a.c. noise suppression and approximately a one-day power reserve, which proved more than adequate to cover any power outages encountered during the experiment.

In addition to saving the data locally with a baler, we used real-time telemetry for all underground sites and six of the nine surface sites. The underground stations were synchronized using a custom-designed GPS optical distribution system. The GPS signal was received by a GPS antenna mounted on the roof of the SURF administration building and piped to a Q330 in



▲ **Figure 1.** (a) Location of the Homestake array. (b) Homestake seismometer array layout. The lines of different colors depict the relevant drifts at various depths, along which we installed underground seismic stations. The black filled circles denote the surface stations (remote surface stations DEAD, SHL, and TPK were located approximately 2–3 km outside the depicted region). The two shafts at the Homestake Mine, known as the Yates and Ross shafts, denoted by black filled reverse triangles, are also shown. The color version of this figure is available only in the electronic edition.



▲ **Figure 2.** (a) Top-down view photograph of the concentric insulation huts erected around the seismometer placed on a granite tile, grouted to the concrete floor. (b) Photograph of one of the underground stations depicting the insulating hut on the right and a black table on the left hosting the necessary power and readout electronics. The color version of this figure is available only in the electronic edition.

the server room of the same building. This master Q330 data logger was used to convert the received high-frequency GPS signal into the separate 1 PPS (1 pulse per second) and National Marine Electronics Association metadata components that were used as an external timing signal for the underground instru-

ments. The output from the master Q330's EXT GPS port was fed into an electro-optical transceiver to convert the analog voltage output to optical signals. The transceivers were custom-made for this application by Liteway, Inc. (model number GPSX-1001). An optical-fiber network of optical splitters and transceivers was installed underground to distribute this GPS timing signal to all underground stations while maintaining its SNR ratio throughout the mine. At each station, a transceiver was used to convert the optical signals back to electrical, which were then sent into the Q330's EXT GPS port. Phase errors logged by the Q330 digitizers suggest the timing precision achieved with this system was of the order of 1  $\mu$ s. Systematic errors from propagation and electronic delays were negligible.

Five of the nine surface stations were located on SURF property above the underground stations. Another station was located at Lead High School (LHS) in collaboration with the Lead-Deadwood Public School District. We deployed the remaining three stations on private land in an outer ring at a nominal radius of 5 km from the array center. We used conventional, portable broadband sensor vaults but carefully separated the wall of the sensor vault from the concrete pad poured at the bottom. This detail is known from early experience in the 1990s at IRIS-PASSCAL to reduce tilt noise from soil motions. All but one of the sites (DEAD in Deadwood, South Dakota) were bedrock sites with a concrete pad poured on weathered metamorphic rocks of

variable lithologies. The surface stations were all oriented by conventional compass methods, which means the precision is less than the underground sites oriented with the Octans instrument. We insulated the sensor vault with a layer of foam and burial with as much of a soil cover as possible. We had the common problem of rain washing some cover away that we restored when the instruments were serviced.

Whereas the three outer stations were stand alone, the remaining six inner stations all used radio telemetry. Of these, the LHS site located near the high school used a point-to-point radio that linked the outdoor site to a Linux computer in a computer laboratory at the school. The remaining five stations were radio-linked to a master radio on the roof of the SURF administration building where our data logging computer was located. All surface sites except LHS used solar power; LHS used an a.c. system similar to underground sites but with a larger battery backup. All surface sites used the standard Q330 GPS timing system.

The telemetry system we deployed used a computer running the Antelope software (e.g., [Malone, 1999](#); [Boulder Real Time Technologies \[BRTT\], 2017](#)) at the SURF administration building to handle real-time communication to all underground sites and five of the nine surface sites. We ran a separate Linux computer running Antelope at LHS to handle real-time communications with that single site. This approach was necessary to deal with firewall issues at both SURF and the high school. We then set up an orb2orb feed to a University of Minnesota computer that acted as a data concentrator. The participating institutions and the IRIS-DMC were then able to tap that connection for real-time feeds with a latency of a few tens of seconds. We developed a custom monitoring system to automatically test for a range of conditions and build web-based quality control summaries. We also set up a rotating shift schedule among our group members to monitor this diagnostic information on a daily basis. This allowed us to quickly identify and diagnose problems. This was a major factor in the very high data recovery rate of this experiment (near 100% for every site except DEAD, which had power problems in the winter of 2015–2016 but was otherwise operational). Furthermore, the telemetry data have no inertial mass position-related issues except for two sensors failures (ORO was replaced in April 2015 and 800 in April 2016). In addition, this quality control monitoring allowed us to detect and diagnose a subtle problem on station E2000. This station began showing odd tilt transients, which were tracked down to failure of the thinset grout on the base of one of our granite tiles. This was repaired in May 2015 by pouring a new concrete pad and setting the tile directly on the concrete.

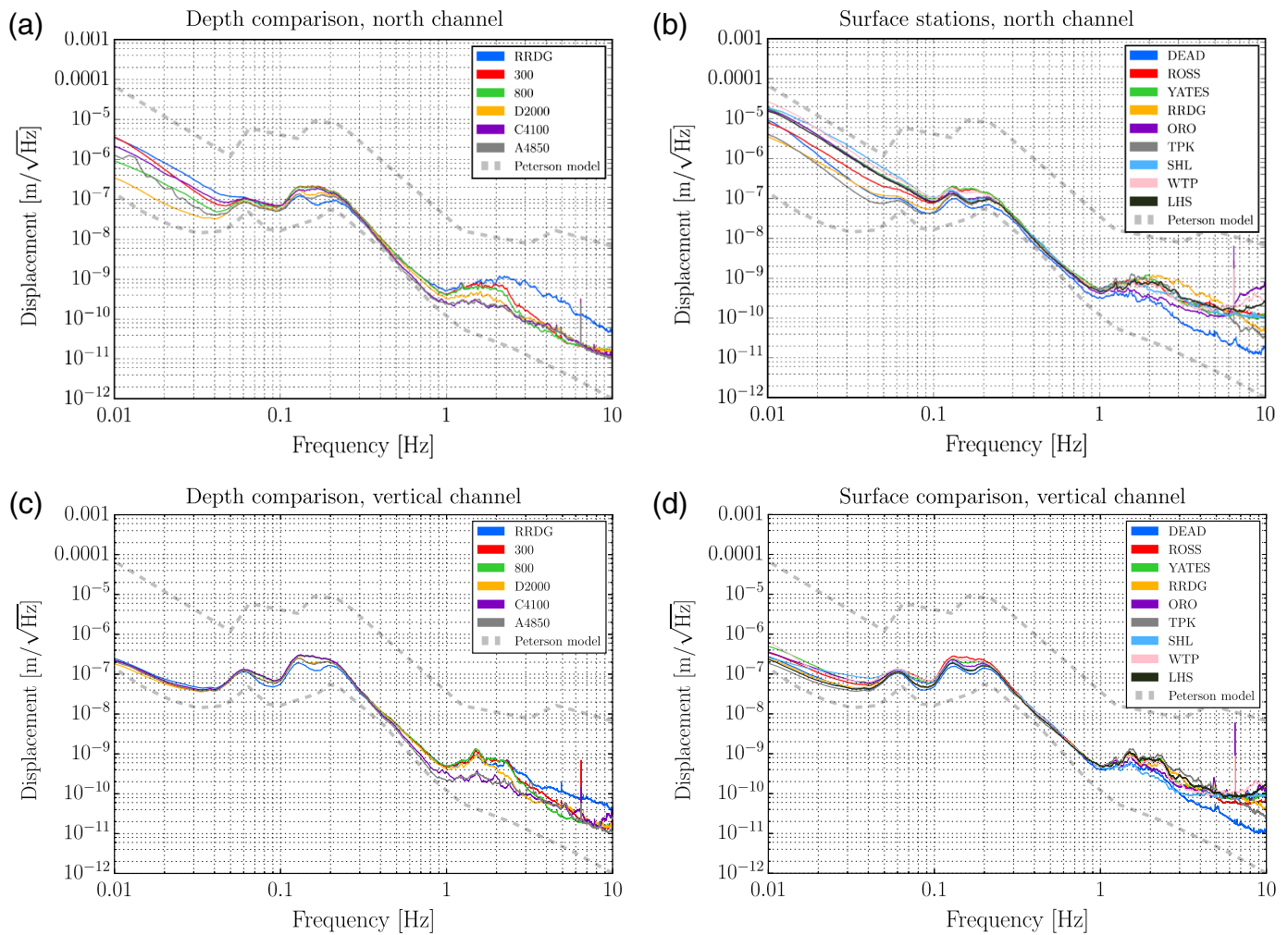
## PRELIMINARY RESULTS

The primary novelty of the Homestake Array is that it is a 3D broadband array, spanning a cubic volume that is  $\sim 1.5$  km on each side (volume of  $\sim 3.4$  km<sup>3</sup>), in a relatively seismically quiet region. This unusual array configuration leads to both unique opportunities and challenges. Here, we provide preliminary analyses that demonstrate some of the potential prospects

and issues. We first describe the ambient noise levels of the stations in our array, which at some periods are exceptionally low. We then describe seismic events detected with our array that demonstrate the kinds of event data that were collected in this experiment. As expected for an array of such small aperture, waveforms have a very high degree of coherence, but there are subtle differences between stations at depth and those nearer to the surface that suggest more detailed analysis may yield fruitful information regarding near-surface heterogeneity and free surface conversion of waves. Finally, because the results presented here represent only initial work on this dataset, we discuss possible future applications of these data.

## Noise Spectra

The ambient seismic noise levels at the Homestake Mine, especially at the deepest levels, are remarkably low and stable over the lifespan of our array. We demonstrate this by computing the displacement amplitude spectral density (ASD) of seismic noise over long periods for different stations and for different seismic channels (east, north, and vertical). We use all available data (from January 2015 to December 2016), split into 900-s intervals, including all known transients. The median amplitudes in each frequency bin for the north–south and vertical seismic channel are shown in Figure 3a,b and 3c,d, respectively in comparison with the low- and high-noise models of [Peterson \(1993\)](#). Figure 3a compares the north–south ASDs for stations at several different depths. All of the stations are in close agreement in the middle range of frequencies (0.1–0.5 Hz), which corresponds to the microseismic peak. At higher frequencies, there is significantly less noise with depth: above 0.5 Hz, the stations at 4100 and 4850 ft depths are nearly an order of magnitude quieter than other stations. At the lowest frequencies ( $< 0.1$  Hz), there is also a good agreement between the stations, although a slight increase in noise is apparent at the surface stations; this may be due to larger temperature variations closer to the surface that induce tilts in the concrete pads. Although the underground stations at any given depth tend to agree very well, there is a wide range of variability among the surface stations, as depicted in Figure 3b. This is due to differences in the local environment of the surface stations and in their proximity to human activity: although YATES and ROSS were near the two shafts of the mine (and therefore subject to constant activity), ORO was far from human activity. Similarly, although ORO was located in a valley and shielded by nearby topography, RRDG was located at the top of a bare hill and subject to strong winds. Similar patterns are observed in the vertical channels (Fig. 3c,d). There is also a considerable difference between the vertical and the horizontal channels at low frequencies. At 0.01 Hz, the vertical channels on all stations have almost an order of magnitude lower noise than the horizontals because of tilt noise that increases with period on horizontal components ([Wielandt, 2002](#)). Although tiltmeters could be used to identify and suppress tilt noise in the seismic data, they were not available in this array. On the other hand, compared with surface sites, the horizontal components of all the underground sites are very quiet.



▲ **Figure 3.** Median amplitude spectral densities (ASDs) for Homestake seismic stations. Numbered legend entries denote depth in feet, and numberless legend entries denote surface stations. Peterson low- and high-noise models are shown as dashed lines. (a) North–south horizontal channel data at various depths. (b) North–south horizontal channel data at surface sites. (c) Vertical channel data at various depths. (d) Vertical channel data at the surface sites. The color version of this figure is available only in the electronic edition.

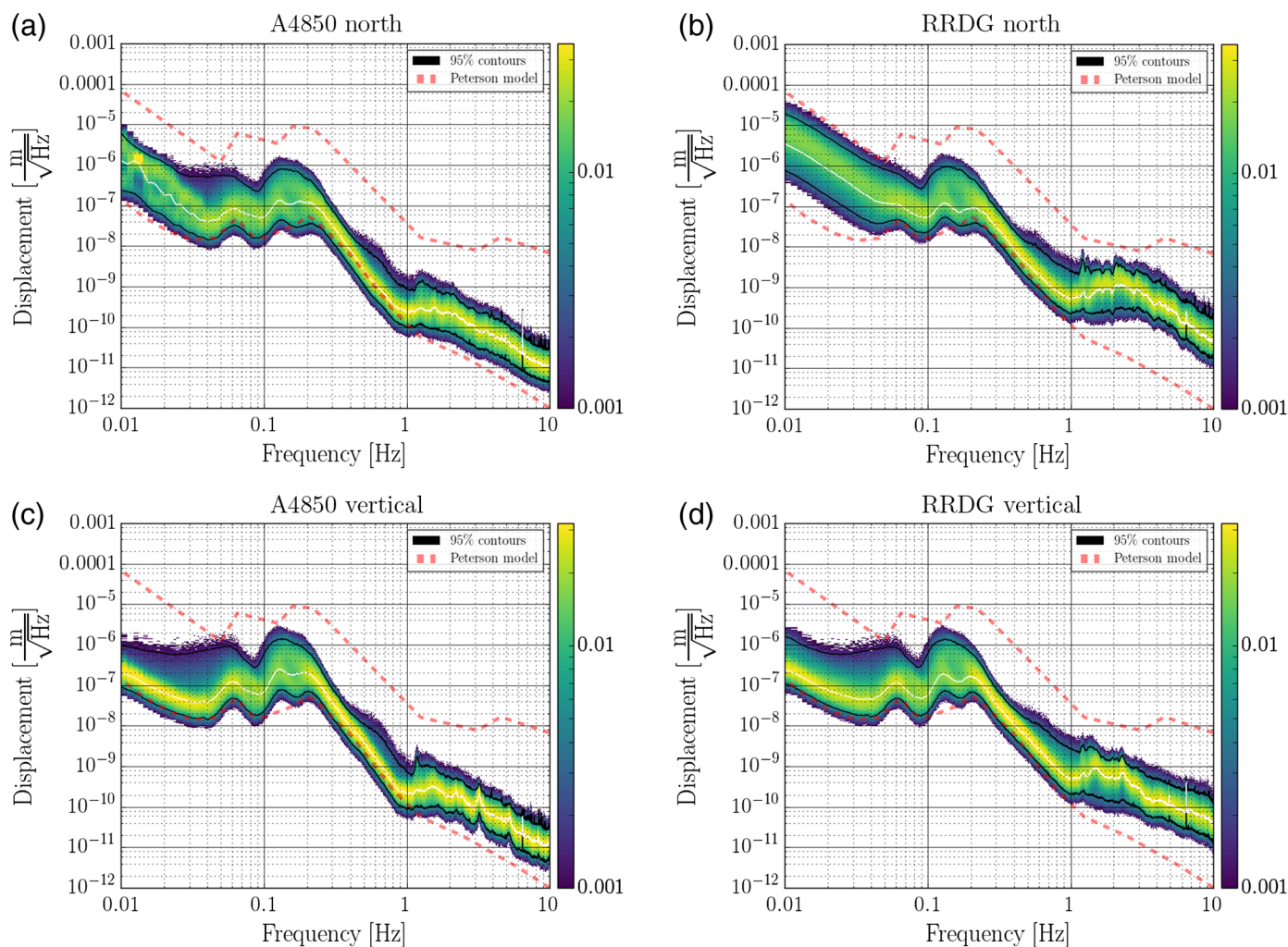
Figure 4a,b shows ASD histograms for the A4850 underground station and for the RRDG surface station (respectively) as examples of a representative surface station and our deepest and most isolated underground station. The histograms display about 2 orders of magnitude of variation across all frequencies for both the RRDG station and the A4850 station. The A4850 station measures less noise overall and appears to have less variation than RRDG. There also appears to be significantly more high-frequency noise in the RRDG station, potentially caused by wind-generated or anthropogenic surface waves that are suppressed with depth. Both stations stay within the low- and high-noise Peterson models most of the time. However, in the 0.3- to 0.9-Hz range, the A4850 station is actually below the low-noise model a significant fraction of the time. Similar patterns are observed in the vertical channels, as depicted in Figure 4c,d.

The low-noise levels of a significant fraction of our stations at depth suggest that the array may be useful for better understanding how ambient noise levels depend on depth and

in particular what fraction of the noise is spatially and temporally coherent. Such a study, which cannot be done with a single borehole seismic station, is beyond the scope of this contribution but is expected to be discussed in future contributions.

### Event Detection and Waveform Observations

Detecting and analyzing seismic events in an area with otherwise sparse station coverage using our small-aperture array of 24 quiet sites was technically challenging because conventional automated detectors typically assume all sites provide equally weighted independent data. Thus, attempts at automatic detection using Antelope 5.6 (Malone, 1999; BRTT, 2017) applied to our array data augmented by data from eight regional stations (see Fig. 5b) with default parameters resulted in a large number of spurious detections. We solved this issue and reduced the false detection rate to near zero by running the detection algorithm only on the three outer surface sites (DEAD, TPK, and SHL), one of the quietest underground sites (D4850), and the eight regional stations.

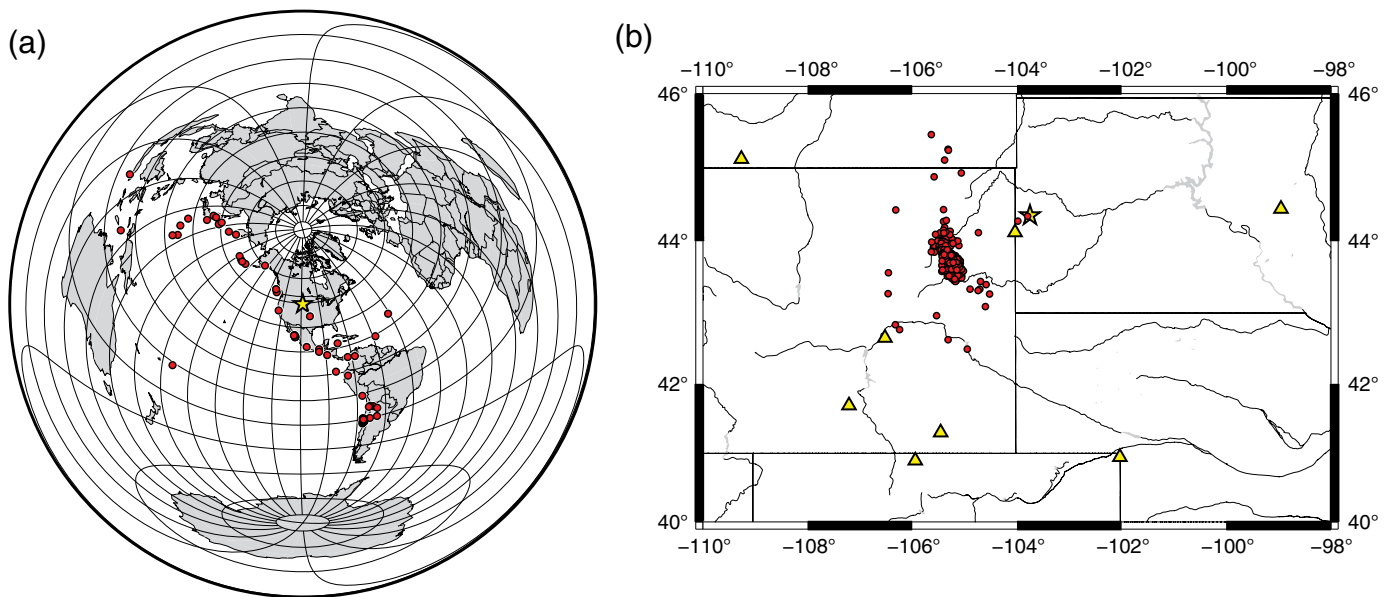


▲ **Figure 4.** Histograms of ASD in the horizontal north–south direction, in each frequency bin (a) for an underground station at 4850 ft depth and (b) for a surface station, calculated from 900 s intervals over more than 1 yr in each frequency bin. Median ASDs (solid white, identical to those shown in Fig. 3), 95% confidence intervals for each frequency bin (solid black), and Peterson low- and high-noise models (dashed) are shown. The color scale shows the overall distribution. Panels (c,d) are the same as (a,b) but for the vertical channels, respectively. The color version of this figure is available only in the electronic edition.

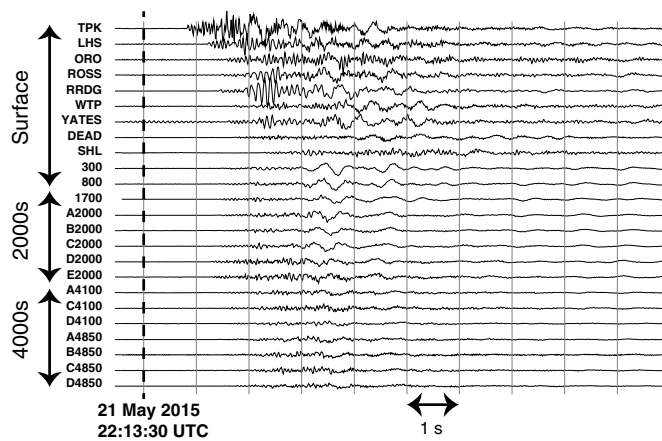
Because our focus was not on detection but on signal characteristics, we focused initially on the largest signals. We thus required six *P*-wave associations before declaring an event. These choices resulted in significantly raising the detection threshold and no longer detecting events from a local active surface mine, located only 2.5 km west of station TPK. A large number ( $\sim 1$  per workday) of such very local events exist (see e.g., Fig. 6) and could be analyzed in future studies. For example, Figure 6 clearly shows the theoretically expected suppression of Rayleigh waves with depth, with Rayleigh waves barely visible on any of the stations in the 4000s subarray. These local events have potential for testing models for Rayleigh-wave propagation in an anisotropic medium.

We completed a standard analyst review of the revised detection routine applied to six months of data (1 July 2015–31 December 2015), resulting in the estimated event locations shown in Figure 5. Of the 431 epicenters, 359 are in the area shown in Figure 5b. Figure 5a shows 72 events at regional to

teleseismic distances that could not be accurately located with this array alone. The locations shown in Figure 5a are epicenters estimated by the U.S. Geological Survey (Array Network Facility [ANF], 2017). In contrast, the locations in Figure 5b were estimated with the dbgenloc program (Pavlis *et al.*, 2004) assuming the IASPEI91 earth model. All of the 359 local events in Figure 5b are likely to be coal-mining explosions from the Powder River basin in eastern Wyoming, roughly 100 miles away from Homestake. All have similar waveform characteristics, with emergent *P* waves and prominent surface waves with a dominant period of 1–2 s. Phase-velocity measurements show the first arrival for all of these events are *P<sub>g</sub>*, as expected for their distance from the array. Despite assuming fixed depths (of zero), some epicenters were poorly constrained and likely badly mislocated because too few of the regional stations had observable *P* or *S* waves. Most well-located events cluster in the coal mining district, supporting our hypothesis that these are mining related.



▲ **Figure 5.** Epicenter maps of events recorded by the Homestake 3D array. (a) An azimuthal equal distance projection map centered at the array site marked with a star. Epicenters of distant earthquakes recorded by the array in the 2015 study period are shown as circles. (b) Epicenter map focused on local and regional events. The array location is again shown as a star and estimated event epicenters are shown as circles. Triangles are regional stations used for detection and location of the events plotted. The color version of this figure is available only in the electronic edition.

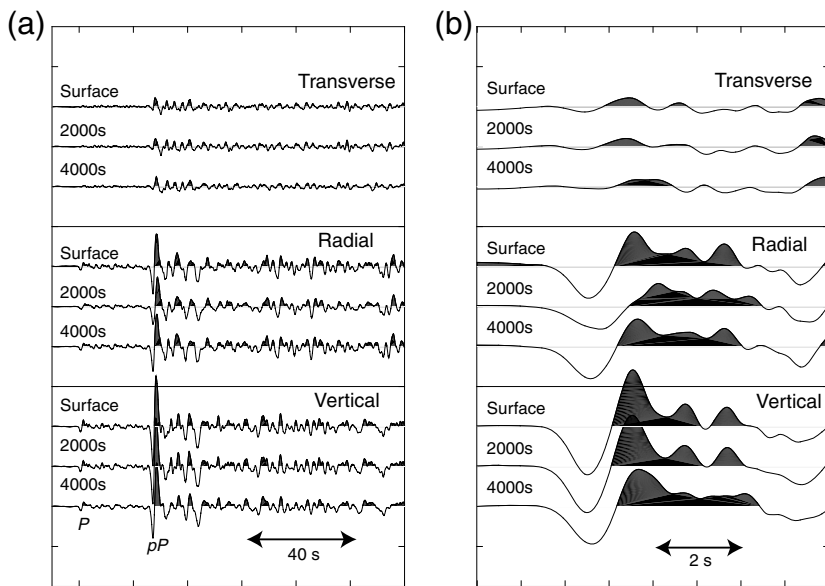


▲ **Figure 6.** Vertical-component seismograms from a local surface mine event. Seismograms are displayed at true amplitude and grouped by subarrays used throughout this article. Records for each subarray are sorted by epicentral distance from the estimated source location (~4 km west of TPK). Subarrays are ordered by increasing depth.

Figures 7 and 8 show three-component subarray stacks for two representative events. Because we found systematic differences in waveforms with sensor depth, these subarray stacks were grouped into three subarrays defined in Figure 6 (Surface, 2000s, and 4000s). We treated the 300 and 800 stations as part of the Surface subarray, grouped the 1700 station with the five 2000-level stations in the 2000s subarray, and grouped the 4100 and 4850 stations in the 4000s subarray. Such

systematic differences are expected because of near-surface effects that have been known to complicate seismic array processing since the early VELA UNIFORM experiments of the 1960s (Green, 1965; Capon *et al.*, 1969; Husebye and Ruud, 1989). To produce each subarray stack, we used an array-based cross-correlation algorithm to align signals prior to stacking (Pavlis and Vernon, 2010). Typical correlation window lengths were 2–4 s for the local mining blasts and 10–20 s for the teleseismic events. The stacked signals of the 3 subarrays were then manually aligned to produce the figures shown.

Figure 7 shows subarray stacks from an intermediate depth event in Alaska, where the *pP* phase is significantly bigger than *P*. Nonetheless, the *P* signal shown magnified in Figure 7b has a very high SNR ratio and a relatively high-frequency content for a teleseism. Figure 8 shows comparable results for a typical, larger Powder River basin mining explosion. The subarray stacks show significant differences in waveforms that are unquestionably not related to background noise. Figure 8 shows a secondary amplitude effect not seen in the teleseismic waveforms. In particular, there is a strong change in amplitude with depth, with the average surface-station *P* wave roughly a factor of 2 higher amplitude than the 4000s subarray average. A comparable difference in *P*-wave amplitude is not seen for the teleseismic signal in Figure 7. How much of that difference is due to differences in emergence angle (steep angle of incidence for the teleseism but approximately horizontal for the mining explosion) and how much of the difference is due to frequency content (upper limit ~2 Hz for the teleseism and upper limit near the 40-Hz antialiasing frequency corner for the mining explosion) is not yet clear.



▲ **Figure 7.** Velocity seismograms from an Alaskan earthquake recorded by the Homestake 3D array (according to the Alaska Earthquake Information Center, the earthquake took place on 29 July 2015 (210) 2:35:59.40000, at 59.8935° N, 153.1962° W, depth = 119.3 km). (a) The three components of subarray stacks defined in the Preliminary Results section. The first 2 min of the data following the *P*-wave signal are shown. These data were filtered with a 0.01- to 2-Hz band-pass filter before stacking. The *P* wave of this event is much smaller than the *pP* phase seen ~25 s after *P* (angular distance on the sphere is 33°). (b) A shorter time window focused on only the *P* wave (13 s following measured *P* time). All plots are true amplitude, meaning amplitude differences between seismograms are real. In all figures, the seismograms have been aligned by cross correlation before stacking. Stacks are aligned manually.

These results, although preliminary and exploratory, further demonstrate the potential of the Homestake array dataset to be used to explore the role of near-surface structure in complicating earthquake waveforms. Unlike surface arrays, in which the complexity of near-surface structure is convolved with complexity of earthquake sources, the Homestake array's geometry allows for separate evaluation of these two aspects of earthquake waveform modeling. Although some of this separation is possible with single borehole arrays, the linear geometry inherent in such arrays is a clear drawback, leading to significant underdetermination of inversions, to which the Homestake array data should be less susceptible.

## CONCLUSIONS AND FUTURE DIRECTIONS

We described a 3D array of high-sensitivity broadband seismometers in the Homestake Mine, South Dakota, spanning roughly a cubic mile underground. We have also shown preliminary results of analyses of data acquired by this array. The data are characterized by exceptionally low seismic noise levels that are also very stable over a year-long time scale. The data also contain high SNR records of hundreds of transient signals due to local or regional mining blasts, to teleseismic events, and to active excitation experiments performed at the surface and underground

that will be described in a separate publication. A preliminary look at these transient events reveals rich structure in terms of depth dependence of different wave components and in terms of interaction of waves with the surface.

We further expect the unusual array geometry to be useful for a number of analyses in addition to the two examples provided. Several such studies are already underway, and here we briefly describe some of these possibilities, which will be subjects of future publications.

In the analysis of ambient noise, the depth extent of the array may be useful in helping estimate the directionality and modal content of the seismic noise. For example, the depth dependence of the Rayleigh and Love eigenfunctions can be directly measured from Homestake data and then used as a constraint on the observed seismic noise modes. Combined with other radiometer-based techniques used in other areas of physics (Thrane *et al.*, 2009), such estimates would directly contribute to the design of future underground gravitational-wave detectors.

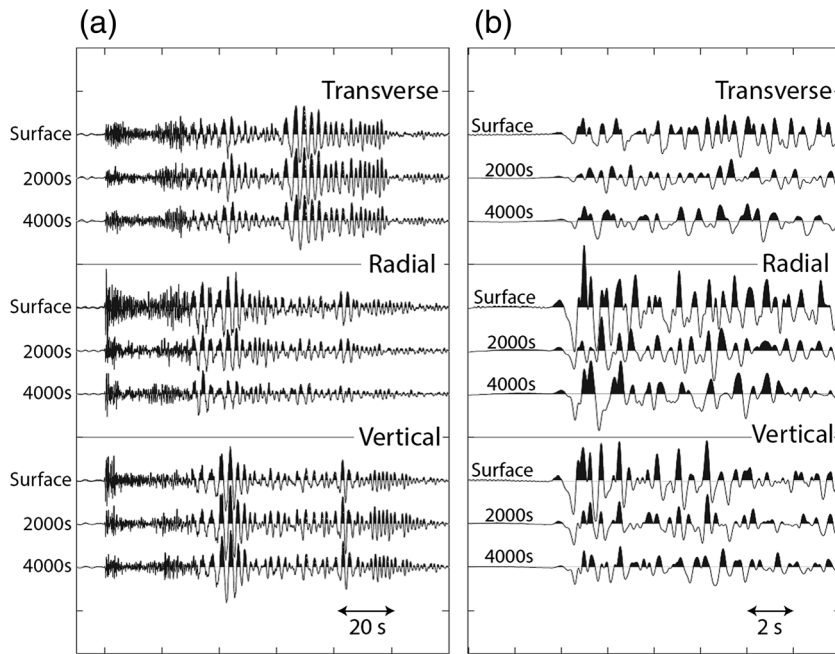
For teleseismic earthquake analysis, other analyses beyond what was described in this article may help understand the scattering and reflection of the nearly vertical incoming waves off of the surface, hence directly measuring the impact of the surface weathered layer on the teleseismic waveforms. One example that is being pursued relates to how well one station's waveforms can be predicted based on knowledge of all

other stations' data. The dependence of station location on the success of such predictions should provide valuable information about the heterogeneity of subsurface structure.

Finally, comparison of *P*-wave particle motions within the array may yield unique data on *P*-wave anisotropy. The rocks at Homestake are predominately highly foliated phyllites and schist (e.g., Noble *et al.*, 1949; Slaughter, 1968) and are known to be highly anisotropic (e.g., Pariseau and Duan, 1989; Johnson *et al.*, 1993; Pariseau *et al.*, 1995a,b, 1996). It is thus not surprising that most of the events we have examined (e.g., Figs. 7 and 8) show significant amplitudes on the transverse component, even during the first cycle of the *P* wave. Further analysis will be necessary to fully identify how strongly anisotropy affects observed waveforms.

## DATA AND RESOURCES

Data collected by the Homestake array and presented here are available at the Incorporated Research Institutions for Seismology (IRIS) Data Management Center available at [www.iris.edu](http://www.iris.edu) (last accessed July 2018) in 2018, designation X6. Also used are data for the array network facility of USArray website available at <http://anf.ucsd.edu/events/> (last accessed April 2017). ✉



▲ **Figure 8.** Seismograms from a typical Powder River basin coal mining explosion recorded by the Homestake 3D array (the explosion origin time estimate is 9 August 2015 20:08:38.62300 UTC, with coordinates 43.7473° N, 105.2149° W, and solution depth fixed at 0 km). All data shown in this figure were filtered with a five-pole Butterworth filter with a passband from 0.25 to 10 Hz. (a) Two min of data following the *P* wave (directly comparable to Fig. 7a). (b) Subarray stacks for 12 s of data following the measured *P*-wave time (directly comparable to Fig. 7b). All figures show seismograms in true amplitude and seismograms were again aligned by a mix of cross correlation and manual picks as described in the Preliminary Results section. Note the strong change in amplitude with depth that is not observed in the teleseismic event shown in Figure 7.

## ACKNOWLEDGMENTS

The authors thank the staff at the Sanford Underground Research Facility and Program for the Array Seismic Studies of the Continental Lithosphere (PASSCAL) for assistance, particularly the help of Tom Regan, Jaret Heise, Jamey Tollefson, and Bryce Pietzyk. Terry Stigall made important technical contributions to operate and maintain the array. The authors also thank C. Langston and an anonymous reviewer for comments. The seismic instruments used for this array were provided by the Incorporated Research Institutions for Seismology (IRIS) through the PASSCAL Instrument Center at New Mexico Tech. Data collected are available through the IRIS Data Management Center. The facilities of the IRIS Consortium are supported by the National Science Foundation under Cooperative Agreement EAR-1261681 and the Department of Energy (DOE) National Nuclear Security Administration. This work was supported by National Science Foundation INSPIRE Grant PHY1344265.

## REFERENCES

Abbott, B. P., R. Abbott, T. D. Abbott, M. R. Abernathy, F. Acernese, K. Ackley, C. Adams, T. Adams, P. Addesso, R. X. Adhikari, and

(The LIGO Scientific Collaboration and Virgo Collaboration), *et al.* (2016a). Observation of gravitational waves from a binary black hole merger, *Phys. Rev. Lett.* **116**, 061102.

- Abbott, B. P., R. Abbott, T. D. Abbott, M. R. Abernathy, F. Acernese, K. Ackley, C. Adams, T. Adams, P. Addesso, R. X. Adhikari, and (The LIGO Scientific Collaboration and Virgo Collaboration), *et al.* (2016b). GW151226: Observation of gravitational waves from a 22-solar-mass binary black hole coalescence, *Phys. Rev. Lett.* **116**, 241103.
- Abbott, B. P., R. Abbott, T. D. Abbott, M. R. Abernathy, K. Ackley, C. Adams, P. Addesso, R. X. Adhikari, V. B. Adya, C. Affeldt, *et al.* (2017). Exploring the sensitivity of next generation gravitational wave detectors, *Classical Quant. Grav.* **34**, 044001.
- Abercrombie, R. E. (1995). Earthquake locations using single-station deep borehole recordings: Implications for microseismicity on the San Andreas fault in southern California, *J. Geophys. Res.* **100**, 24,003–24,014.
- Array Network Facility (ANF) (2017). *Array Network Facility of USArray Website*, available at <http://anf.ucsd.edu/events/> (last accessed April 2017).
- Boore, D. M., and W. B. Joyner (1997). Site amplifications for generic rock sites, *Bull. Seismol. Soc. Am.* **87**, 327–341.
- Boulder Real Time Technologies (BRTT) (2017). *Boulder Real Time Technologies Website*, available at <http://brtt.com> (last accessed April 2017).
- Canuel, B., S. Pelisson, L. Amand, A. Bertoldi, E. Cormier, B. Fang, S. Gaffet, R. Geiger, J. Harms, D. Holleville, *et al.* (2016). MIGA: Combining laser and matter wave interferometry for mass distribution monitoring and advanced geodesy, *Proc. of SPIE 9900: Quantum Optics*, 990008, doi: [10.1117/12.2228825](https://doi.org/10.1117/12.2228825).
- Capon, J., R. J. Greenfield, and R. T. Lacoss (1969). Long-period signal processing results for the large aperture seismic array, *Geophysics* **34**, no. 3, 305–329.
- Ekström, G., and R. W. Busby (2008). Measurements of seismometer orientation at USArray Transportable Array and backbone stations, *Seismol. Res. Lett.* **79**, 554–561.
- Forbes, C. B. (1965). The LASA sensing system design, installation, and operation, *Proc. IEEE* **53**, no. 12, 1834–1843.
- Gaffet, S., J. Wang, M. Yedlin, G. Nolet, D. Brunel, A. Cavallou, D. Boyer, C. Sudre, and M. Auguste (2009). A 3D broadband seismic array at LSBB, *IRIS Data Services Newsletter*, Vol. 11, 6, available at <http://ds.iris.edu/ds/newsletter/vol11/no3> (last accessed July 2018).
- Gibowicz, S. J., R. P. Young, S. Talebi, and D. J. Rawlence (1991). Source parameters of seismic events at the underground research laboratory in Manitoba Canada: Scaling relations for events with moment magnitude smaller than  $-2$ , *Bull. Seismol. Soc. Am.* **81**, 1157–1182.
- Green, P. E. (1965). Principles of an experimental large aperture seismic array (LASA), *Proc. IEEE* **53**, no. 12, 1821–1833.
- Harms, J., F. Acernese, F. Barone, I. Bartos, M. Beker, J. F. J. Van Den Brand, N. Christensen, M. Coughlin, R. DeSalvo, S. Dorscher, *et al.* (2010). Characterization of the seismic environment at the Sanford Underground Laboratory, South Dakota, *Classical Quant. Grav.* **27**, 225011.
- Husebye, E. S., and B. O. Rudd (1989). Array seismology: Past, present, and future developments, in *Observational Seismology*, J. J. Litchiser (Editor), University of California Press, Berkeley, California, 123–153.
- Incorporated Research Institutions for Seismology (IRIS) (2017). *Incorporated Research Institutions for Seismology Metadata Aggregator Website*, available at [www.iris.edu/mda](http://www.iris.edu/mda) (last accessed July 2017).
- Johnson, J. C., W. G. Pariseau, D. F. Scott, and F. M. Jenkins (1993). In situ stress measurements near the Ross shaft pillar, Homestake

- Mine, South Dakota, *Bureau of Mines Report of Investigations, RI 9446*, 1–17.
- Lay, T., and T. C. Wallace (1995). *Modern Global Seismology*, Academic Press, San Diego, California.
- Levin, F. K., and R. D. Lynn (1958). Deep-hole geophone studies, *Geophysics* **23**, 639–664.
- Ma, K.-F., Y.-Y. Lin, S.-J. Lee, J. Mori, and E. E. Brodsky (2012). Isotropic events observed with a borehole array in the Chelungpu fault zone, Taiwan, *Science* **337**, 459–463.
- Malone, S. (1999). Seismic network recording and processing systems I, *Seismol. Res. Lett.* **70**, 175–178.
- McNamara, D. E., and R. P. Buland (2004). Ambient noise levels in the continental United States, *Bull. Seismol. Soc. Am.* **94**, 1517–1527.
- Nadeau, R. M., and T. V. McEvilly (1997). Seismological studies at Parkfield V: Characteristic microearthquake sequences as fault-zone drilling targets, *Bull. Seismol. Soc. Am.* **87**, 1463–1472.
- Noble, J. A., J. O. Harder, and A. L. Slaughter (1949). Structure of a part of the northern Black Hills and the Homestake Mine, Lead, South Dakota, *Geol. Soc. Am. Bull.* **60**, no. 2, 321–352, doi: [10.1130/0016-7606\(1949\)60\[321:SOAPOT\]2.0.CO;2](https://doi.org/10.1130/0016-7606(1949)60[321:SOAPOT]2.0.CO;2).
- Okada, Y., S. Hori, K. Obara, S. Sekiguchi, H. Fujiwara, and A. Yamamoto (2004). Recent progress of seismic observation networks in Japan—Hi-net, F-net, K-NET and KiK-net, *Earth Planets Space* **56**, xv–xxviii.
- Pariseau, W. G., and F. Duan (1989). Finite element analyses of the Homestake Mine study stope; an update, *Proc. 3rd Intl. Symposium on Numerical Models in Geomechanics (NUMOG III)*, Elsevier Appl. Sci., London, United Kingdom, 566–576.
- Pariseau, W. G., J. C. Johnson, M. M. McDonald, and M. E. Poad (1995a). Rock mechanics study of shaft stability and pillar mining, Homestake Mine, Lead, SD; 1. Premining geomechanical modeling using UTAH2, *Bureau of Mines Report of Investigations, RI 9531*.
- Pariseau, W. G., J. C. Johnson, M. M. McDonald, and M. E. Poad (1995b). Rock mechanics study of shaft stability and pillar mining, Homestake Mine, Lead, SD; 2. Mine measurements and confirmation of premining results, *Bureau of Mines Report of Investigations, RI 9576*, 1–20.
- Pariseau, W. G., J. C. Johnson, M. M. McDonald, and M. E. Poad (1996). Rock mechanics study of shaft stability and pillar mining, Homestake Mine, Lead, SD; Part 3 of 3. Geomechanical monitoring and modeling using UTAH3, *Bureau of Mines Report of Investigations, RI 9618*, 1–27.
- Pavlis, G. L., and F. L. Vernon (2010). Array processing of teleseismic body waves with the USArray, *Comput. Geosci.* **36**, no. 7, 910–920.
- Pavlis, G. L., F. L. Vernon, D. Harvey, and D. Quinlan (2004). The generalized earthquake location (GENLOC) package: A modern earthquake location library, *Comput. Geosci.* **30**, 1079–1091.
- Peterson, J. (1993). Observations and modeling of seismic background noise, *U.S. Geol. Surv. Open-File Rept. 93-322*, Albuquerque, New Mexico, 1–42.
- Punturo, M., M. Abernathy, F. Acernese, B. Allen, N. Andersson, K. Arun, F. Barone, B. Barr, M. Barsuglia, M. Beker, et al. (2010). The third generation of gravitational wave observatories and their science reach, *Classical Quant. Grav.* **27**, 084007.
- Richardson, E., and T. Jordan (2002). Seismicity in deep gold mines of South Africa: Implications for tectonic earthquakes, *Bull. Seismol. Soc. Am.* **92**, 1766–1782.
- Rost, S., and C. Thomas (2002). Array seismology: Methods and applications, *Rev. Geophys.* **40**, 1008.
- Saccorotti, G., B. Di Lieto, F. Tronca, C. Fischione, R. Scarpa, and R. Muscente (2006). Performances of the UNDERground SEISmic array for the analysis of seismicity in Central Italy, *Ann. Geophys.* **49**, 17.
- Slaughter, A. L. (1968). The Homestake Mine, in *Ore Deposits of the United States, 1933–1967*, J. D. Ridge (Editor), Vol. 2, American Institute of Mining and Metallurgy, Petroleum Engineers, New York, New York, 1436–1459.
- Stein, S., and M. Wysession (2003). *An Introduction to Seismology, Earthquakes, and Earth Structure*, Blackwell Publishing, Malden, Massachusetts.
- Thrane, E., S. Ballmer, J. D. Romano, S. Mitra, D. Talukder, S. Bose, and V. Mandic (2009). Probing the anisotropies of a stochastic gravitational-wave background using a network of ground-based laser interferometers, *Phys. Rev. D* **80**, 122002.
- Wielandt, E. (2002). Seismic sensors and their calibration, in *New Manual of Seismological Observatory Practice (NMSOP)*, P. Bormann (Editor), Vol. 1, Chap. 5, IASPEI, Potsdam, Germany.

**Vuk Mandic**  
**Tanner Prestegard**  
**Patrick Meyers**  
*School of Physics and Astronomy*  
*University of Minnesota*  
*116 Church Street SE*  
*Minneapolis, Minnesota 55455 U.S.A.*  
**vuk@umn.edu**

**Victor C. Tsai**  
**Daniel C. Bowden**  
*Seismological Laboratory*  
*California Institute of Technology*  
*1200 E. California Boulevard, MS 252-21*  
*Pasadena, California 91125 U.S.A.*

**Gary L. Pavlis**  
**Ross Caton**  
*Department of Geological Sciences*  
*Indiana University*  
*1001 E. 10th Street*  
*Bloomington, Indiana 47405 U.S.A.*

Published Online 22 August 2018